

# Photocatalytic Degradation Mechanism of the Pharmaceutical Agent Salbutamol Using the Mn-Doped TiO<sub>2</sub> Nanoparticles Under Visible Light Irradiation

Yumatorn Mingmongkol, Assadang Polnok, Patcharaporn Phuinthiang, Duangdao Channei, Khakhanang Ratananikom, Auppatham Nakaruk,\* and Wilawan Khanitchaidecha\*



Cite This: <https://doi.org/10.1021/acsomega.3c01776>



Read Online

ACCESS |



Metrics & More

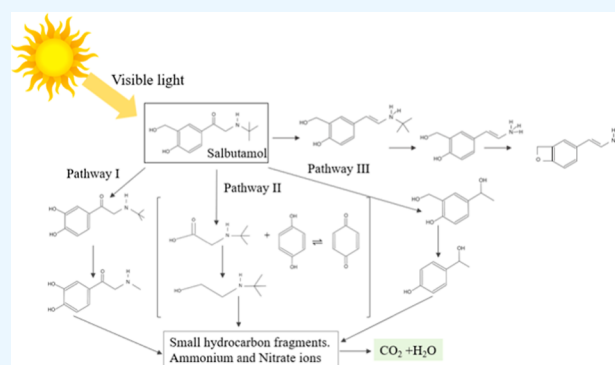


Article Recommendations



Supporting Information

**ABSTRACT:** In the present work, the photocatalytic degradation of salbutamol [2-(*tert*-butylamino)-1-(4-hydroxyl-3-hydroxymethylphenyl)ethanol] under visible irradiation using Mn-doped TiO<sub>2</sub> is investigated. The Mn-doped TiO<sub>2</sub> nanoparticles were synthesized by the sol–gel method with ratios of 0.1, 0.2, and 0.3%. Significant characteristics, including the rutile/anatase phases ratio, specific surface area, and band gap energy, were due to the amount of Mn doping; the narrowest band gap energy of 2.80 eV was observed in 0.2% Mn-doped TiO<sub>2</sub> with specific surface areas of 89.36 m<sup>2</sup>/g and 10.87/89.13 of rutile/anatase phases. The investigation involved salbutamol photocatalytic degradation, a kinetic study, and the identification of intermediate compounds. The results indicated that 0.2% Mn-doped TiO<sub>2</sub> obtained the best salbutamol removal of 95% under an irradiation time of 180 min. Salbutamol slowly degraded to the intermediate compounds in the first 60 min ( $k = 0.0088$  1/min), and these intermediate compounds were dramatically mineralized to small hydrocarbon fragments and carbon dioxide in the later irradiation times ( $k = 0.0179$  1/min). According to the high-performance liquid chromatography–mass spectrometry (HPLC–MS) results, possible degradation pathways of salbutamol were proposed: 2-(*tert*-butylamino)-1-(3,4-dihydroxyphenyl)ethanone, 2-(*tert*-butylamino)-ethanol, and 2-(*tert*-butylamino)-1-(4-hydroxyl-3-hydroxymethylphenyl)ethanone were initially formed and then transformed to 2-(methylamino)-1-(3,4-dihydroxyphenyl)ethanone, 2-(*tert*-butylamino)-acetic acid, hydroquinone, and 1-(4-hydroxyphenyl)ethanol, respectively. The mineralization of all intermediate compounds was verified by 90% chemical oxygen demand (COD) reduction, and the effluent contained a relatively low COD concentration of 7.8 mg/L.



## 1. INTRODUCTION

Pharmaceuticals are chemical compounds used to cure disease and improve health. During the last few decades, drug consumption has increased from individual households to hospitals and livestock farms. Various pharmaceutical compounds, including antibiotics, anti-inflammatory drugs, beta-blockers, and steroids, have recently been detected in wastewater, water resources, and drinking water.<sup>1</sup> In 2019, a wide range of concentration (115–9054 ng/L) of sulfamethoxazole was detected in the influent of a wastewater treatment plant, and around 55–97 ng/L of ibuprofen was reported in drinking water.<sup>1</sup> In the meantime, paracetamol and gemfibrozil, with maximum values of 1204 and 152 ng/L, respectively, were found in estuaries in China.<sup>2</sup> Although the low concentration of pharmaceutical compounds was observed in the aquatic environment, the concentration can increase along the food chain and have cascading effects on the human health and ecosystem, such as change in enzyme activities, alternation in growth rate and reproduction, and reduced abundance and diversity.<sup>3</sup>

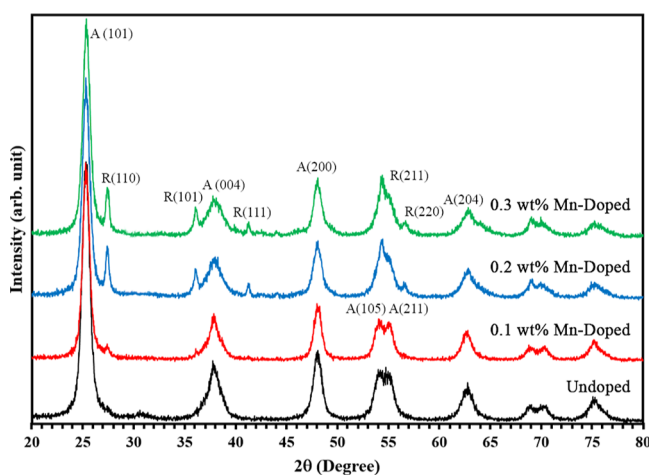
Salbutamol, [2-(*tert*-butylamino)-1(4-hydroxy-3-hydroxymethylphenyl) ethanol], also known as albuterol, is the most widely used drug for relieving the acute symptoms of asthma. Due to its anti-asthmatic effect, this chemical is able to increase muscle proteins, reduce total body fat, and promote muscle growth. The use of salbutamol in sports has been forbidden due to its anabolic-like effects and central nervous system effects.<sup>4</sup> In addition, salbutamol is illegally used as feed additives for growth promotion in cattle, pigs, and other farm animals.<sup>5</sup> Salbutamol has a high potential to be excreted in urine as an unchanged drug and its conjugated metabolite, as well as in pharmaceutical wastewater discharge. Salbutamol is soluble in water. Henry's

Received: March 16, 2023

Accepted: April 19, 2023

**Table 1. Summary of Pharmaceutical Degradation by the Photocatalysis Process in Literature**

| pharmaceuticals | concentration (mg/L) | catalysts                            | loading (g/L) | time (min) | light source          | degradation efficiency (%) | references |
|-----------------|----------------------|--------------------------------------|---------------|------------|-----------------------|----------------------------|------------|
| paracetamol     | 5                    | ZnO                                  | N/A           | 240        | visible               | 54                         | [12]       |
| paracetamol     | 5                    | Ag-doped ZnO                         | N/A           | 240        | visible               | 92                         | [12]       |
| paracetamol     | 80                   | Ag-doped AgO                         | 0.1           | 20         | microwave irradiation | 26                         | [13]       |
| tetracycline    | 8888                 | Bi <sub>2</sub> WO <sub>6</sub>      | 1.0           | 60         | visible               | 60                         | [14]       |
| tetracycline    | 8888                 | AgBr/Bi <sub>2</sub> WO <sub>6</sub> | 1.0           | 60         | visible               | 87                         | [14]       |
| carboplatin     | 20                   | TiO <sub>2</sub> P25                 | 0.5           | 30         | UV-A                  | 72                         | [15]       |
| salbutamol      | 15                   | TiO <sub>2</sub> P25                 | 0.5           | 30         | UV                    | 87                         | [4]        |

**Figure 1.** XRD patterns of undoped TiO<sub>2</sub>, 0.1, 0.2, and 0.3% Mn-doped TiO<sub>2</sub> nanoparticles.

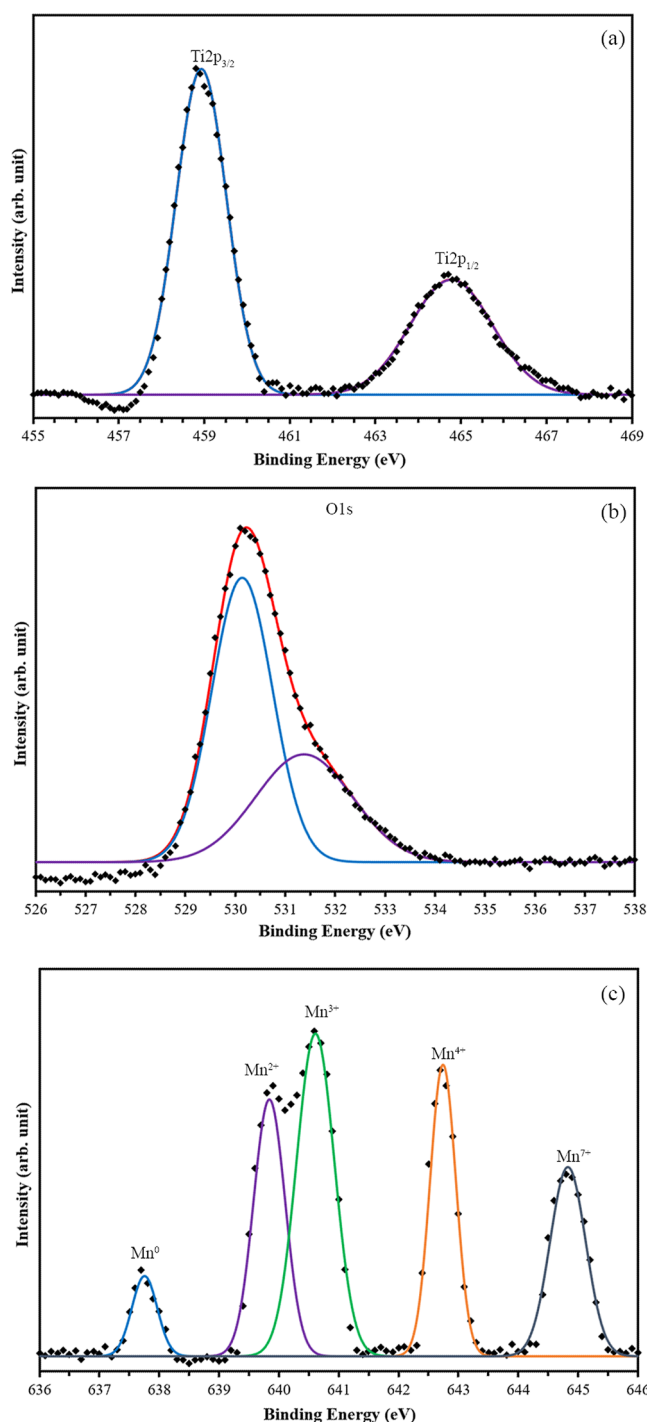
law constant of  $5 \times 10^{-14}$  atm·m<sup>3</sup>/mol (at 20 °C) and sorption coefficient of  $\log K_{OC} -1.6$  to  $-1.15$  indicate that hydrolysis is

**Table 2. Percentage of Anatase and Rutile Phases of Mn-Doped TiO<sub>2</sub>**

| Mn-doped TiO <sub>2</sub> (wt %) | peak area |        | percentage |        |
|----------------------------------|-----------|--------|------------|--------|
|                                  | anatase   | rutile | anatase    | rutile |
| undoped                          | 1382.63   | 31.27  | 97.79      | 2.21   |
| 0.10                             | 923.12    | 59.22  | 93.97      | 6.03   |
| 0.20                             | 1105.84   | 134.90 | 89.13      | 10.87  |
| 0.30                             | 1051.05   | 132.44 | 88.81      | 11.19  |

unlikely to be a significant depletion mechanism, volatilization is generally slow, and it is not likely to adsorb to soil sediment.<sup>4</sup>

In recent years, new technologies for the decomposition of organic micropollutants in the aqueous environment have been developed. Photocatalysis, one of the most advanced oxidation processes, is capable of achieving organic and inorganic substance degradation, including pharmaceuticals such as paracetamol, tetracycline, carboplatin, and salbutamol, as summarized in Table 1. Among metal oxide photocatalysts, TiO<sub>2</sub> is considered the top candidate due to its environmental friendliness, photocorrosion resistance, chemical stability, availability, and low cost. However, there are some limitations of pure TiO<sub>2</sub>, such as the wide band gap (3.2 eV for anatase), which leads TiO<sub>2</sub> to work under UV irradiation, and a high electron/hole recombination rate, which reduces the photocatalytic activity for degrading pollutants.<sup>6</sup> In addition, sunlight containing 3–5% UV and 42–43% visible light is naturally more sustainable than other energy sources. The enhancement of TiO<sub>2</sub> photocatalytic activity under visible irradiation has been reported in literature such as TiO<sub>2</sub>/cellulosic fibers<sup>7</sup> and silver

**Figure 2.** XPS spectra of 0.2 wt % Mn-doped TiO<sub>2</sub> nanoparticles; (a) Ti 2p, (b) O 1s, and (c) Mn 2p.

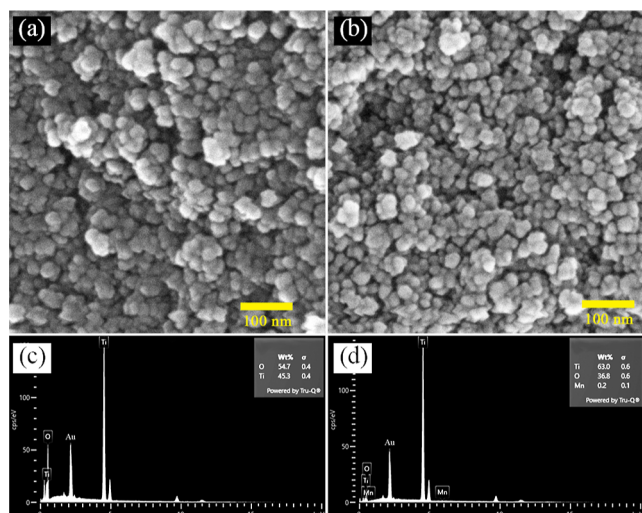


**Figure 3.** SEM images of (a) undoped TiO<sub>2</sub>, (b) 0.2% Mn-doped TiO<sub>2</sub>, and EDX spectra of (c) undoped TiO<sub>2</sub>, (d) 0.2% Mn-doped TiO<sub>2</sub> nanoparticles.

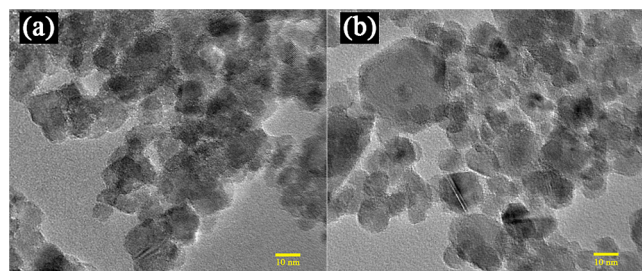


**Figure 4.** TEM images of (a) undoped TiO<sub>2</sub> and (b) 0.2% Mn-doped TiO<sub>2</sub> nanoparticles.

**Table 3.** Surface Morphology Properties and Band Gap Energy of Undoped and Mn-Doped TiO<sub>2</sub>

| Mn-doped TiO <sub>2</sub> (wt %) | SSA (m <sup>2</sup> /g) | average particles size (nm) | band gap energy (eV) |
|----------------------------------|-------------------------|-----------------------------|----------------------|
| undoped                          | 77.22                   | 9.88 ± 1.17                 | 2.92                 |
| 0.1                              | 120.16                  | 9.92 ± 1.03                 | 2.91                 |
| 0.2                              | 89.36                   | 9.88 ± 1.22                 | 2.80                 |
| 0.3                              | 79.65                   | 9.89 ± 1.07                 | 2.88                 |

and cerium co-doped mesoporous TiO<sub>2</sub>.<sup>8</sup> Doping noble-metal nanoparticles, such as Ag,<sup>9</sup> Au,<sup>10</sup> and Pd,<sup>11</sup> is an alternative approach to increase photoabsorption of TiO<sub>2</sub> in the visible region; the doped metals penetrate the bulk of the nanoparticles and/or reside on the surface. However, the above metal nanoparticles are expensive, which makes them unfavorable for large-scale production.

In this work, manganese (Mn) was selected as a metal dopant to improve the photocatalytic activity under visible light and reduce the electron/hole recombination rate of TiO<sub>2</sub>. The Mn-doped TiO<sub>2</sub> nanoparticles were synthesized using a sol-gel process and characterized for its significant physico-chemical properties using X-ray diffraction (XRD), X-ray photoelectron spectroscopy (XPS), scanning electron microscopy (SEM), transmission electron microscopy (TEM), and diffuse reflection spectroscopy (DRS) techniques. The photocatalytic activity of visible-driven Mn-doped TiO<sub>2</sub> nanoparticles for salbutamol degradation was evaluated, and its intermediate compounds were clarified.

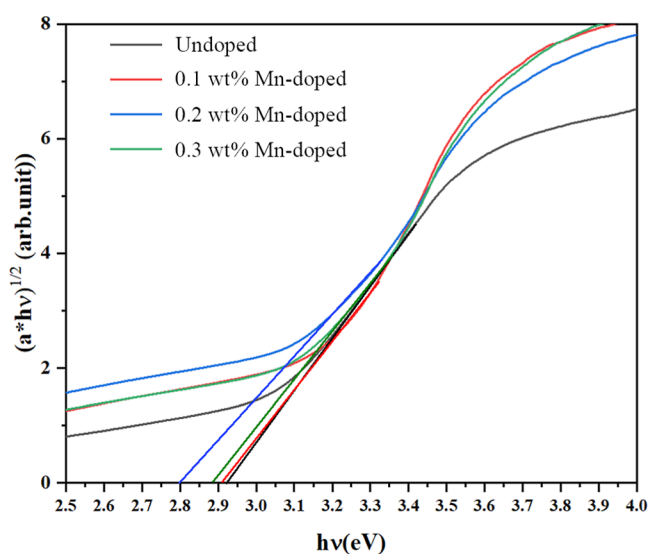


**Figure 5.** Tauc plot of undoped and Mn-doped TiO<sub>2</sub>.

## 2. EXPERIMENTAL SECTION

**2.1. Nanoparticles Synthesis.** Undoped TiO<sub>2</sub> and Mn-doped TiO<sub>2</sub> nanoparticles were prepared by the sol-gel method. 50 mL of titanium(IV)isopropoxide (TTIP: 97% reagent grade, Sigma-Aldrich) was added to 50 mL of 2-propanol (99.8%, RCI Labscan), and the solution was continuously stirred. Various amount of manganese chloride (MnCl<sub>2</sub>·4H<sub>2</sub>O; 98.0%, Ajax Finechem Australia), including 0, 0.029, 0.058, and 0.087 grams, were dissolved in 10 mL of deionized water and added to the TTIP solution. The pH of the mixture was adjusted to 2 by nitric acid (70%, Ajax Finechem Australia). After 4 h of stirring, the mixture was kept at 55 °C for 24 h and calcined at 400 °C for 2 h. Finally, undoped TiO<sub>2</sub>, 0.1, 0.2, and 0.3% Mn-doped TiO<sub>2</sub> were achieved.

**2.2. Nanoparticles Characterization.** The physicochemical properties of undoped TiO<sub>2</sub> and Mn-doped TiO<sub>2</sub> nanoparticles were characterized using the following procedures: crystal structure and phase identification were measured by XRD (Bruker, D2 Phaser) under Cu K $\alpha$  radiation ( $\lambda = 0.154$  nm) and  $2\theta$  ranging from 20 to 80°. The chemical and electronic states of the atoms were identified by XPS (Axis, Ultra DLD, Kratos Analytical). The surface topography and composition were observed using TEM (JEOL—JEM-2100Plus; Japan), SEM (FE-SEM; Apreo S, Thermo Fisher Scientific; USA), and energy-dispersive X-ray (EDX; UltimMax65, Oxford; UK). The average particle size was obtained from TEM images (30 particles per sample) by using ImageJ software. Further, the specific surface areas (SSA) of the nanoparticles were determined by the Brunauer–Emmett–Teller method (BET; Micromeritics, TriStar-II-3020) using nitrogen adsorption-desorption analysis at 77 K, and the optical band gap was calculated using DRS (Shimadzu, UV-360) with an integrating sphere attachment (ISR-3100, Shimadzu; Japan) and a Tauc plot.

**2.3. Photocatalytic Activity Test.** The photocatalytic activity of undoped and Mn-doped TiO<sub>2</sub> was examined in salbutamol solution. The salbutamol solution of 15 mg/L was prepared in deionized water, and the nanoparticles were added at a concentration of 1 g/L. After 60 min in the dark to reach the adsorption equilibrium, the salbutamol solution with nanoparticles was irradiated with 50 W of visible light (Oppl LED

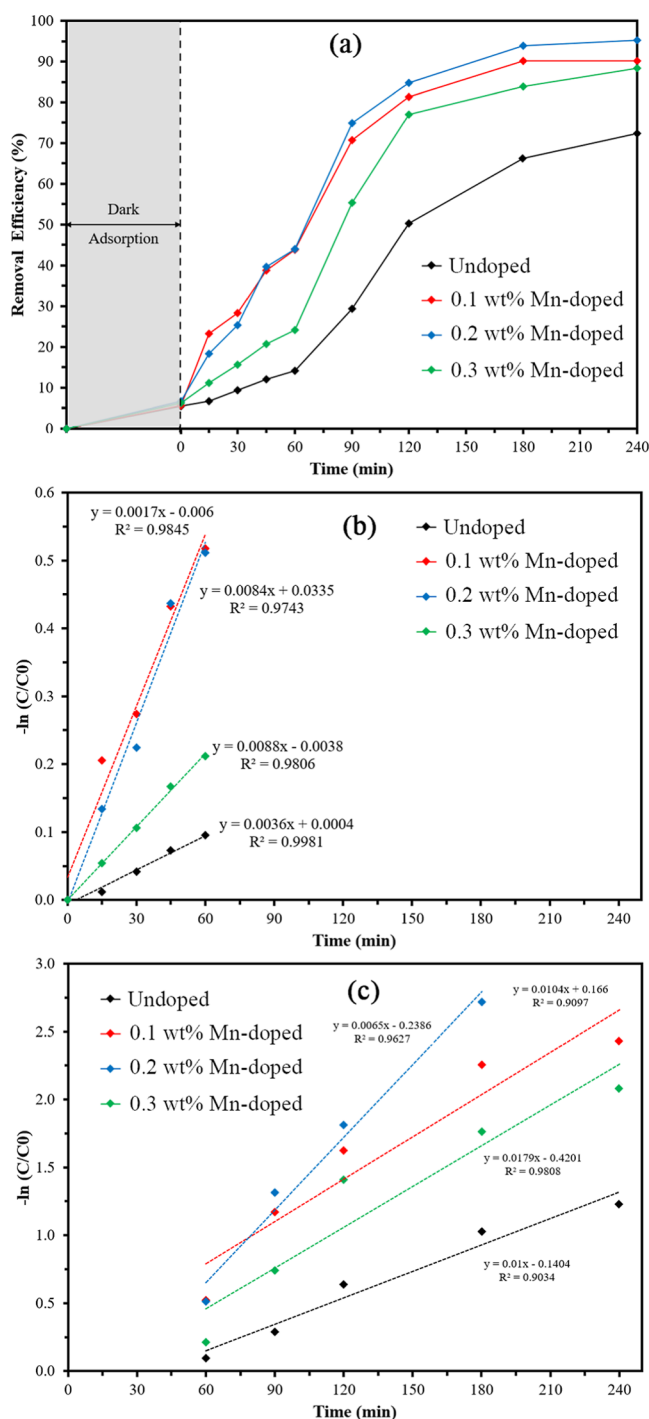


**Figure 6.** Salbutamol degradation of undoped and Mn-doped  $\text{TiO}_2$  under visible irradiation; (a) removal efficiency, (b) kinetic from 0 to 60 min, and (c) kinetic from 60 to 240 min.

4000K, Oppl Lighting Co. Ltd., China) for 240 min with interval sampling every 15 min. The degradation efficiency of salbutamol was measured by UV–vis spectroscopy (UV-6100, Mapada) and compared to the standard calibration plot of absorbance intensity at 276 nm and salbutamol concentration. The salbutamol degradation efficiency was calculated by absorbance reduction at a maximal wavelength of 276 nm. The reaction kinetic of photocatalytic oxidation of salbutamol was calculated by the Langmuir–Hinshelwood kinetic model,<sup>4</sup> as shown in eqs 1 and 2

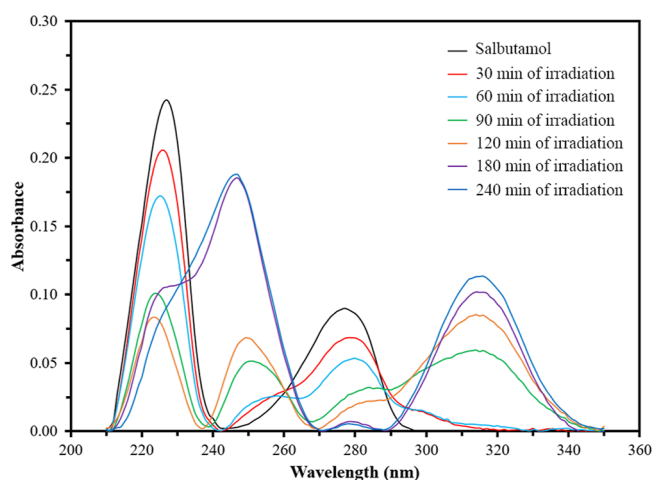


**Figure 7.** Absorbance spectra of salbutamol during photodegradation by 0.2% Mn-doped  $\text{TiO}_2$  under visible irradiation.

$$-r = dC / dt = kKC / 1 + KC \quad (1)$$

where  $r$  is the oxidation rate,  $C$  is the concentration of the reactant,  $t$  is the irradiation time,  $k$  is the reaction rate constant, and  $K$  is the adsorption coefficient of the reactant

$$-\ln \frac{C}{C_0} = kt \quad (2)$$

where  $C_0$  and  $C$  are the concentrations of the reactant at time 0 and  $t$ ,  $t$  is the irradiation time, and  $k$  is the apparent first-order rate constant.

The carbon content in the solution was analyzed by chemical oxygen demand (COD) measurement (5220 B) due to the standard methods for the examination of water and wastewater.<sup>16</sup> Further, the potential intermediates during photocatalytic degradation of salbutamol were identified using high performance liquid chromatography–mass spectrometry (HPLC-MS). The HPLC-MS was performed on an Agilent 1260 infinity series HPLC system (Agilent, Waldron, Germany) coupled with an Agilent 6540 Q-TOF LC–MS spectrometer (Agilent Technologies, Santa Clara, CA, USA). In addition, the C-18 column was used as the Luna C18 column, 4.6 mm  $\times$  150 mm, 5  $\mu\text{m}$  (Phenomenex Inc., Torrance, CA, USA). The mobile phase was 0.1% (v/v) formic acid in the water, mobile phase A, and 50% (v/v) acetonitrile in methanol, mobile phase B. The linear gradient elution was 5–95% for solvent B starting at 0–15 min and post-run for 5 min. The flow rate was 0.5 mL/min, and the injection volume of the sample was 5  $\mu\text{L}$ . Mass Hunter software (Agilent Technologies) controlled all the acquisition and analysis of data. All samples were analyzed in the positive mode to provide information for identification.

### 3. RESULTS AND DISCUSSION

The crystallinity analysis of nanoparticles is shown in Figure 1. The XRD patterns indicate that undoped  $\text{TiO}_2$  consisted of two phases of  $\text{TiO}_2$ , which were anatase and rutile as major and minor phases, respectively. The percentage of rutile/anatase ratio can be calculated using the peak area;<sup>17</sup> the calculating results proved that the presence of Mn in the  $\text{TiO}_2$  structure caused the increase of rutile/anatase ratio in the structure, as presented in Table 2. At 0.2% Mn doping, it provided the significant rutile phase. Theoretically, the rutile phase presents in the  $\text{TiO}_2$  structure at  $\geq 600$   $^\circ\text{C}$ ; however, the calcination

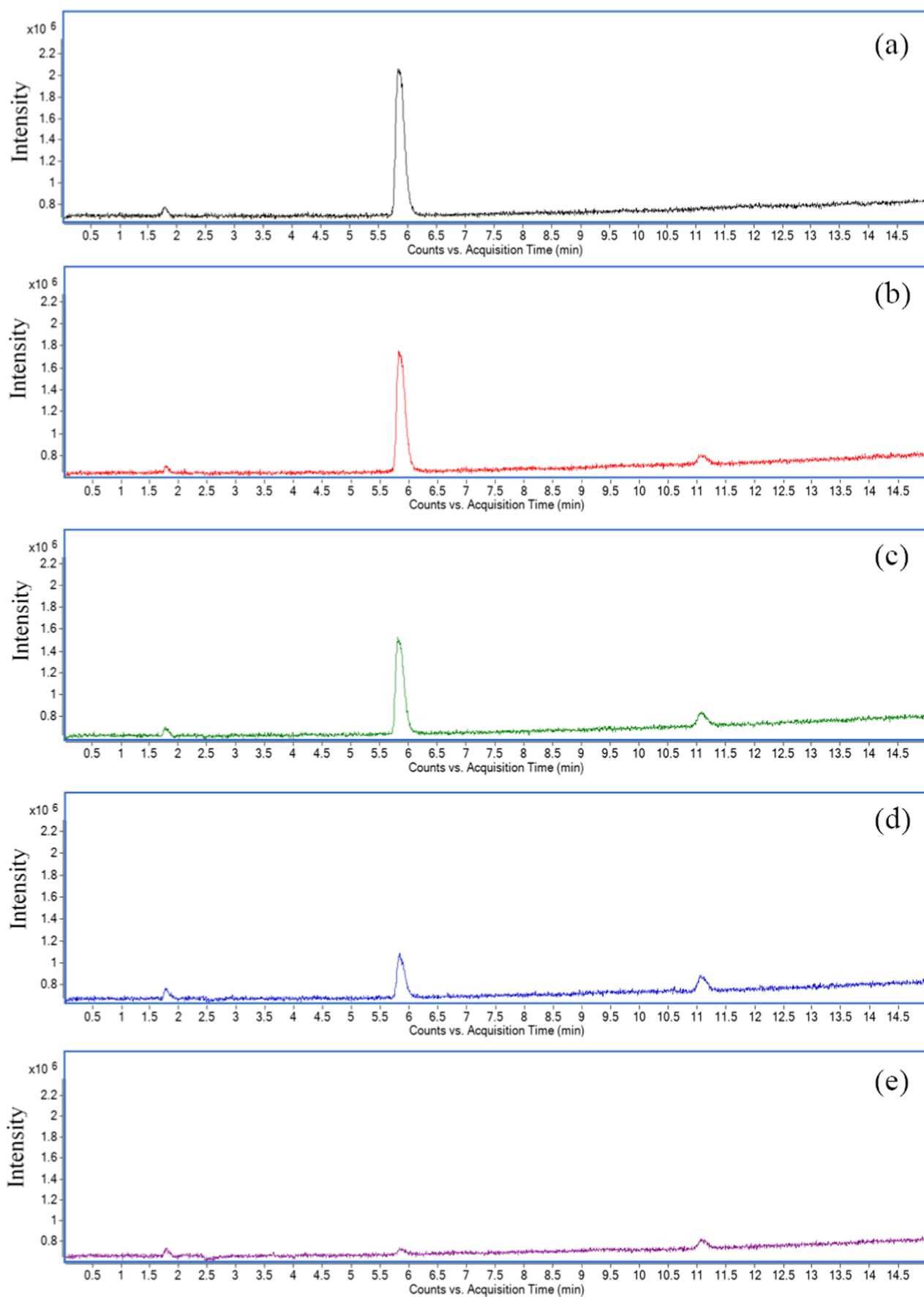


**Figure 8.** HPLC of salbutamol during photodegradation by 0.2% Mn-doped TiO<sub>2</sub>: (a) dark adsorption, (b) 30, (c) 60, (d) 90, and (e) 180 min of visible irradiation.

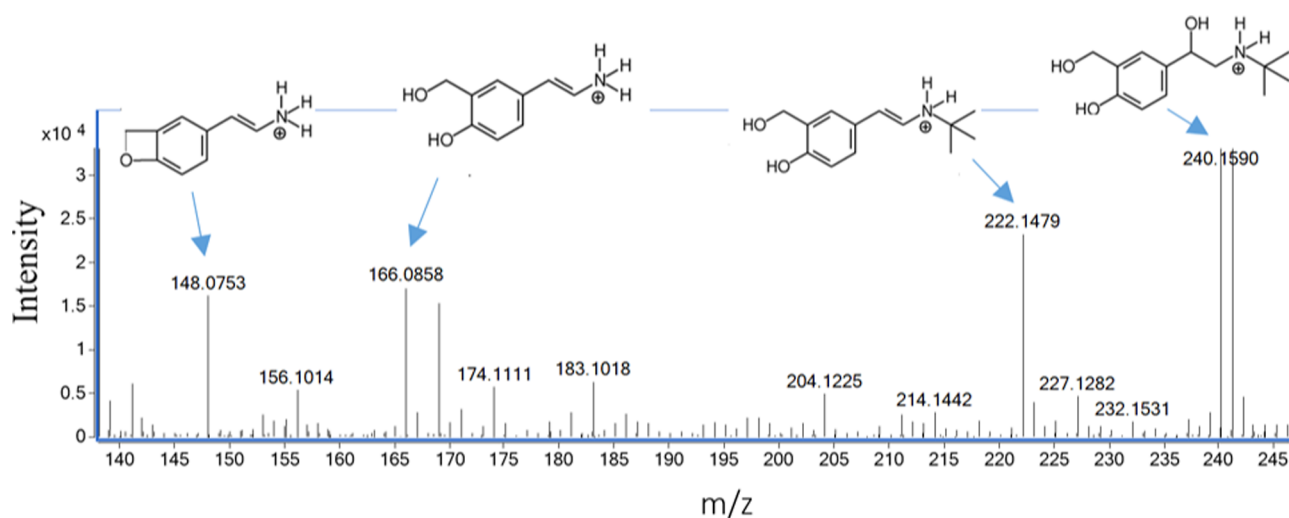


**Figure 9.** HPLC/MS spectra of salbutamol after dark adsorption.

temperature was set at only 400 °C in this work. The explanation of this phenomenon was that Mn was known as a promoter in the TiO<sub>2</sub> structure;<sup>18</sup> then, increasing the Mn doping level caused an increase in the rutile/anatase phase ratio.

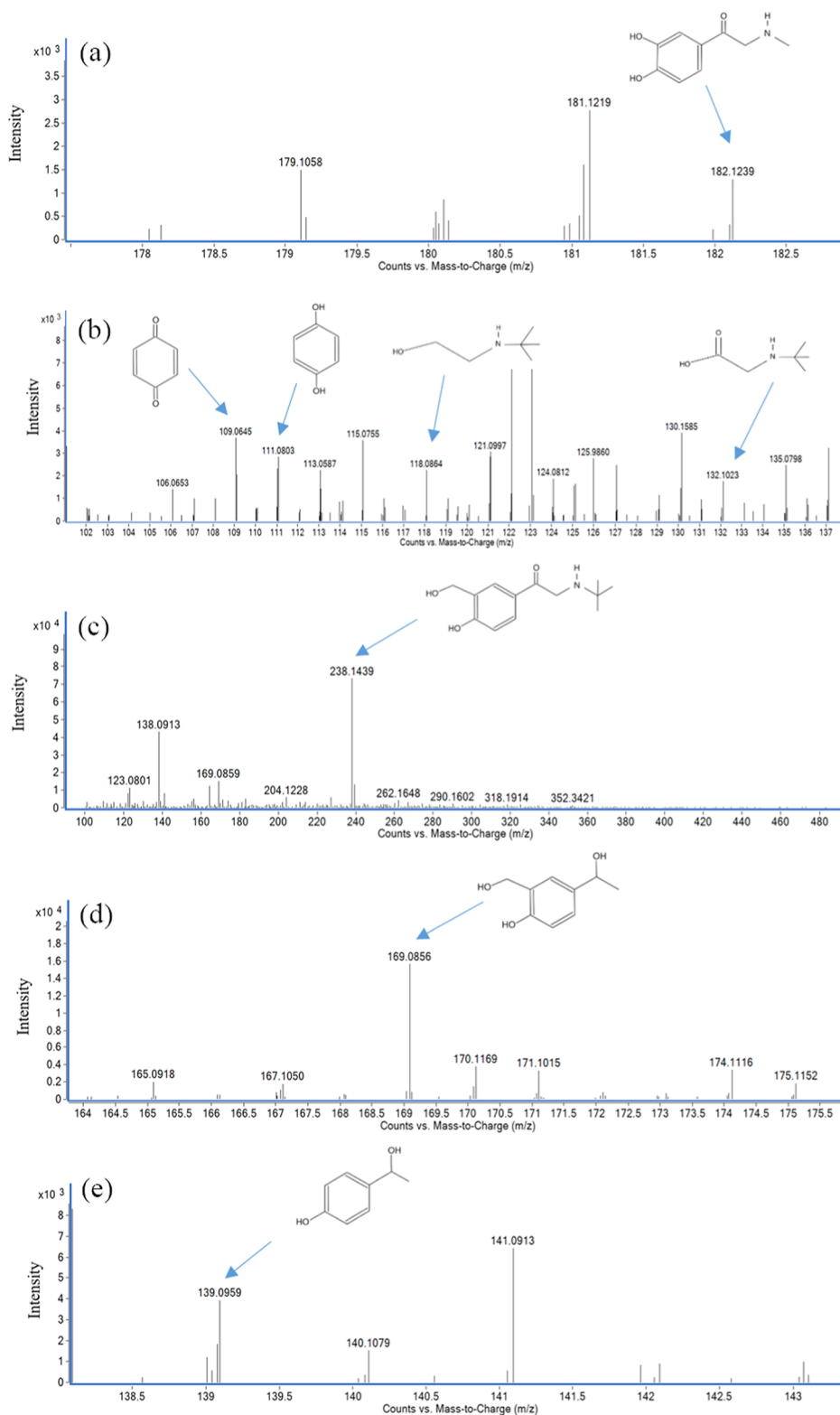
XPS was carried out to investigate the chemical states of atoms in the Mn-doped TiO<sub>2</sub> nanoparticles, as shown in Figure 2. As presented in Figure 2a, the Ti 2p levels of all samples had two symmetrical spin-orbit doublet peaks of Ti 2p<sub>3/2</sub> and Ti 2p<sub>1/2</sub> located at 458.6 and 464.3, which correspond to the Ti<sup>4+</sup> oxidation state. In addition, the binding energy from the XPS spectra of O 1s can be assigned to lattice oxygen at 530.1 eV, oxygen vacancy at 531.0 eV, and adsorbed oxygen on the surface at 532.0 eV.<sup>19</sup> Figure 2c reveals Mn 2p peaks of Mn-doped TiO<sub>2</sub> nanoparticles, which exhibit the XPS peaks from metallic Mn at 637.7 eV<sup>20</sup> and the multivalence of Mn species: Mn<sup>2+</sup> (639.8 eV), Mn<sup>3+</sup> (640.6 eV), Mn<sup>4+</sup> (642.7 eV), and Mn<sup>7+</sup> (644.9 eV). The XPS results prove that Mn can provide multivalence ion in the TiO<sub>2</sub> structure. Based on theoretical predictions, Mn<sup>4+</sup> corresponds to substitutional Mn and the host Ti atoms. On the other hand, the other peaks (Mn<sup>2+</sup>, Mn<sup>3+</sup>, and Mn<sup>7+</sup>) were compatible to the satellite peaks and caused the atomic and/or lattice disorder that results in the increasing rutile/anatase phase ratio. Since Mn is known as a multivalence doping agent and promoter of the rutile phase in the TiO<sub>2</sub> structure; hence, the increasing of ion valences could cause more lattice defects, which leads to the formation of the rutile phase in the structure.

Figure 3a,b shows the surface morphology of undoped and 0.2 wt % Mn-doped TiO<sub>2</sub>. In addition, the EDX spectra of both nanoparticles are also presented in Figure 3c,d. The TEM images were used to confirm the particle size of nanoparticles, and the results indicated that the undoped TiO<sub>2</sub> and 0.2% Mn-doped TiO<sub>2</sub> nanoparticles were spherical shape, as shown in Figure 4a,b, respectively. The size of undoped and Mn-doped nanoparticles were approximately 10 nm, and no significant differences was observed; the statistical analytical data are given in Table S1 and plots of histogram are shown in Figures S1–S4. From EDX spectra, approximately 0.1 wt % of Mn was detected in the Mn-doped TiO<sub>2</sub> nanoparticles, as shown in Figure 3c,d. The SSA of nanoparticles increased with the present of Mn in TiO<sub>2</sub> structure, as shown in Table 3. However, the higher Mn doping levels resulted to decrease the SSA, which is due to the increasing of rutile/anatase phases ratio. Since rutile is known as

larger grain size compare to anatase; therefore, the SSA should be decreasing by increasing the rutile/anatase ratios.

The band gap energy of nanoparticles was calculated based on the Kubelka–Munk relationship using a Tauc plot from the DRS spectra. The tangent's intercept to the curve ( $hw$  vs  $[F(R)hw]^{1/2}$ ) approximates the direct band gap energy, as shown in Figure 5 and summarized in Table 3. The band gap energy of undoped TiO<sub>2</sub> was 2.92 eV, which was lower than that of pure TiO<sub>2</sub> in the literature (3.2 eV). This is due to the combination of anatase and rutile phases that occurred in this work, whereas only the anatase phase was generally observed in the literature.<sup>21,22</sup> Moreover, other characteristic properties, such as particle size, also contributed to the band gap.<sup>23</sup> From Figure 5 and Table 3, the band gap energy of nanoparticles was reduced by Mn doping; the narrowest band gap energy of 2.80 eV, which falls in the visible light region, was in the 0.2% Mn-doped TiO<sub>2</sub>. It also has to be note that at 0.3 wt % of Mn doping concentration, the band gap was increased to 2.88 eV. The explanation of this phenomenon is that at high doping concentrations the Mn ions can cause compressive stress in the lattice; this defect leads to an increase in the band gap.<sup>24</sup>

The photocatalytic degradation of pharmaceutical salbutamol was performed under visible light irradiation. Figure 6a shows that only 5–6% of salbutamol was removed in dark adsorption for all nanoparticles. This is because the negative surface charge of TiO<sub>2</sub><sup>25</sup> and Mn-doped TiO<sub>2</sub><sup>26</sup> has less electrostatic interaction with the negative solvent molecule of salbutamol.<sup>25,27</sup> However, the salbutamol removal efficiency was gradually increasing with irradiation times and achieved 72% in the undoped TiO<sub>2</sub>. Similarly, the highest salbutamol removal efficiency of 95% was observed in the 0.2% Mn-doped TiO<sub>2</sub>, followed by the 0.1% Mn-doped TiO<sub>2</sub> (91% salbutamol removal) and the 0.3% Mn-doped TiO<sub>2</sub> (88% salbutamol removal), respectively. From this result, it can be explained that the Mn ions on the Ti lattice sites generated the narrow band gaps, resulting in high electrons and holes for further photocatalytic oxidation. However, the highest Mn doping of 0.3% caused crystal defects, recombination of electrons and holes, and eventually a decrease in photocatalytic oxidation.<sup>28</sup> Further, the photodegradation kinetic of salbutamol was relatively slow within 60 min ( $k = 0.002–0.008$  1/min), and the photodegradation rate was proportionally increased by increasing irradiation from 60 to 240 min ( $k = 0.007–0.018$  1/

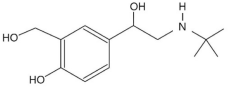
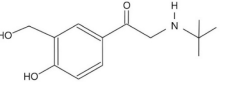
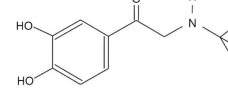
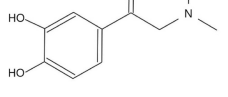
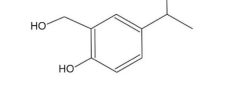
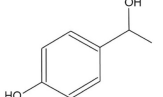
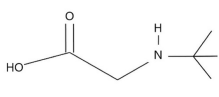
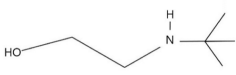
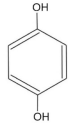
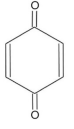


**Figure 10.** Mass spectrum of identified intermediates at various  $m/z$  fragments. (a) 2-(methylamino)-1-(3,4-dihydroxyphenyl)ethanone; (b) 1,4-benzoquinone, hydroquinone, 2-(*tert*-butylamino)-ethanol, and 2-(*tert*-butylamino)-acetic acid; (c) 2-(*tert*-butylamino)-1-(4-hydroxyl-3-hydroxymethylphenyl)ethanone; (d) 1-(4-hydroxyl-3-hydroxymethylphenyl)ethanol; and (e) 1-(4-hydroxylphenyl)ethanol.

min), as shown in Figure 6b,c. These two stages of degradation refer to the degradation of salbutamol into intermediate compounds and the mineralization of intermediates into carbon dioxide and water.

In addition, the results from Figure 7 indicate that the intensity of the salbutamol peak (at 276 nm) gradually decreased within 60 min of irradiation, and the peak was very small after 180 min. However, the peak at 316 nm was suddenly detected in

Table 4. Products during Photocatalytic Degradation of Salbutamol

| m/z<br>[M+H] <sup>+</sup> | t <sub>R</sub><br>(min) | Molecular<br>weight<br>(M <sub>w</sub> ) | Structure  | References. |
|---------------------------|-------------------------|--|--|-------------|
| 240                       | 5.83                    | 239                                      | <br>2-(tert-butylamino)-1-(4-hydroxyl-3-hydroxymethylphenyl)ethanol   | [4, 29]     |
| 238                       | 11.08                   | 237                                      | <br>2-(tert-butylamino)-1-(4-hydroxyl-3-hydroxymethylphenyl) ethanone | [29]        |
| 224                       | 4.64                    | 223                                      | <br>2-(tert-Butylamino)-1-(4-hydroxyl-3-methylphenyl)ethanol          | [4]         |
| 182                       | 4.68                    | 181                                      | <br>2-(Methylamino)-1-(3,4-dihydroxyphenyl)ethanone                  | [4]         |
| 169                       | 6.02                    | 168                                      | <br>1-(4-hydroxyl-3-hydroxymethylphenyl)ethanol                     | [29]        |
| 139                       | 10.36                   | 138                                      | <br>1-(4-hydroxyphenyl)ethanol                                      | [29]        |
| 132                       | 4.73                    | 131                                      | <br>2-(tert-Butylamino)-acetic acid                                 | [4]         |
| 118                       | 6.03                    | 117                                      | <br>2-(tert-Butylamino)-ethanol                                     | [4]         |
| 111                       | 12.46                   | 110                                      | <br>hydroquinone   | [4]         |
| 109                       | 11.63                   | 108                                      | <br>para benzoquinone   | [4]         |

90 min, and its intensity was increasing by increasing irradiation times from 90 to 240 min. The results agreed with the above kinetic explanation of salbutamol degradation to intermediate compounds and their mineralization. According to the HPLC spectra in Figure 8a–e, the main peak of salbutamol was detected at a retention time ( $t_R$ ) of 5.83 min. The salbutamol peak disappeared around 76% in 90 min of irradiation, whereas the other species at approximately  $t_R$  11.83 min reached the maximum; the ratio of  $t_R$  11.83 to  $t_R$  5.83 was kept at about 44%.

The intermediate compounds of salbutamol degradation were determined by HPLC-MS. After dark adsorption, the product ions and protonated salbutamol are shown in Figure 9. The highest intensity ( $1.1 \times 10^6$ ) of protonated salbutamol was found at  $m/z$  240. The protonated salbutamol lost water and formed the product ion at  $m/z$  222; the latter lost isobutene and formed the product ion at  $m/z$  166. The fragment ion  $m/z$  148 was formed by the loss of water from  $m/z$  166. The fragment structures of salbutamol are listed in Figure 9. The intensity of protonated salbutamol at  $m/z$  240 decreased to  $0.9 \times 10^6$  and  $0.8 \times 10^6$  at 30 and 60 min of irradiation times, respectively.

The protonated salbutamol was lost to a methylic group to form 2-(tert-butylamino)-1-(3,4-dihydroxyphenyl)ethanone at  $m/z$  224, and it was then degraded into the species at  $m/z$  182, which was identified as 2-(methylamine)-1-(3,4-dihydroxyphenyl)ethanone. In addition, the lower molecular weights at  $m/z$  109, 110, 118, and 132 were also observed, and they were labeled 1,4-benzoquinone, hydroquinone, 2-(tert-butylamino)-ethanol, and 2-(tert-butylamino)-acetic acid, respectively.<sup>4</sup>

The molecular ion at  $m/z$  238 was recognized as 2-(tert-butylamino)-1-(4-hydroxyl-3-hydroxymethylphenyl)ethanone, which was transformed from the hydroxyl oxidation on the side chain of salbutamol.<sup>29</sup> The molecular ion at  $m/z$  169 was detected as 1-(4-hydroxyl-3-hydroxymethylphenyl)ethanol, which was due to the loss of tert-butylamino. The hydroxymethyl was then lost, and the product of 1-(4-hydroxyphenyl)ethanol was generated at  $m/z$  139. The observation of intermediate products during salbutamol photocatalytic degradation is listed in Figure 10a–e and summarized in Table 4.



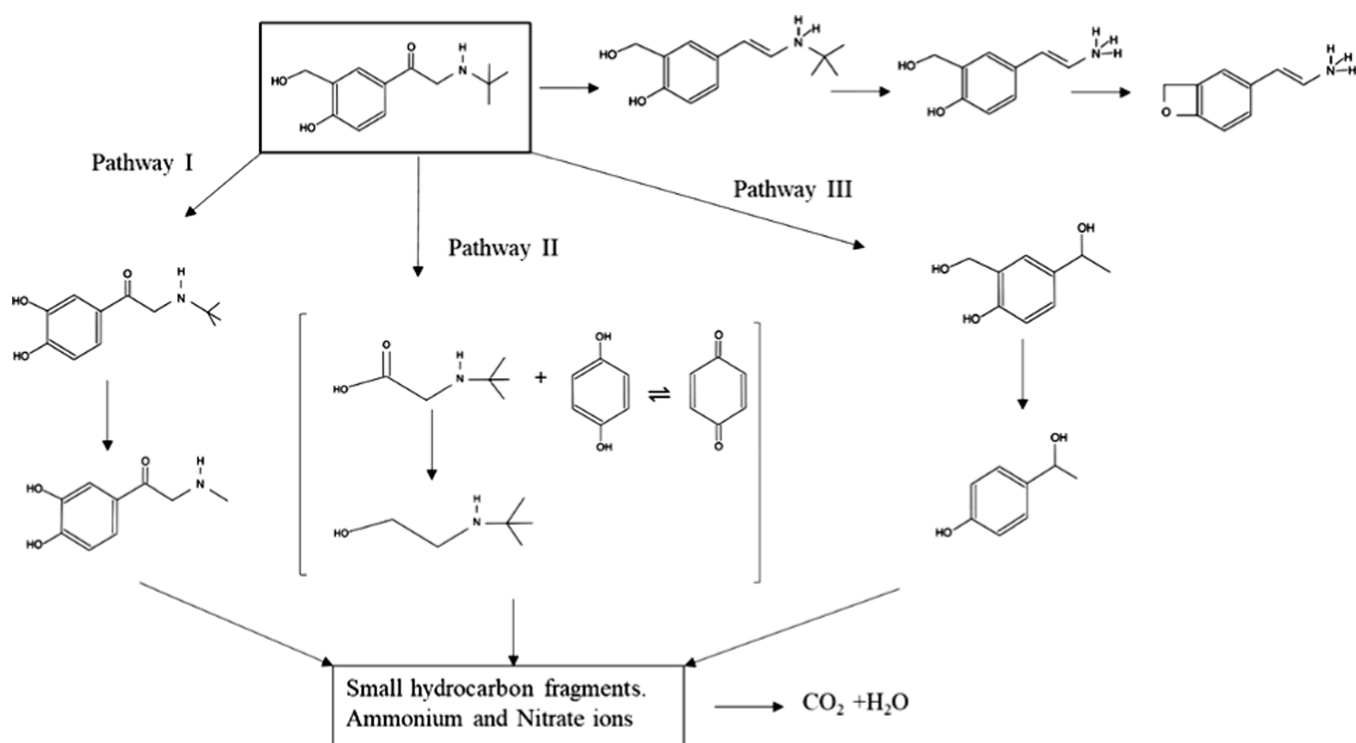


Figure 11. Possible photocatalytic degradation scheme of salbutamol.

From all the above results, the photocatalytic degradation of salbutamol involved the generation of intermediate compounds and their mineralization into carbon dioxide. The mineralization of intermediate products was verified by COD measurement; the COD concentration was approximately 77 mg/L after dark adsorption, and the concentration decreased to 15.5 and 7.8 mg/L after 180 and 240 min irradiations, respectively. The nitrogen in the salbutamol molecule was eventually degraded to ammonium and nitrate ions.<sup>4</sup> The potential photodegradation pathway of salbutamol is presented in Figure 11. The fragments were mainly diols unlike toxic amines and phenols. Therefore, the photocatalytic degradation by 0.2% Mn-doped TiO<sub>2</sub> nanoparticles was a green and eco-friendly technology with rapid and efficient degradation of toxic pharmaceutical, especially salbutamol.

#### 4. CONCLUSIONS

The photocatalytic degradation of salbutamol in the water was studied using Mn-doped TiO<sub>2</sub> nanoparticles with a visible light source. The properties of nanoparticles, including particle size, specific surface area, band gap energy, and crystalline phase, were correlated with the amount of Mn doping. The highest salbutamol removal efficiency of 95% was achieved in the 0.2% Mn-doped TiO<sub>2</sub>, followed by the 0.1 and 0.3% Mn-doped TiO<sub>2</sub> and the undoped TiO<sub>2</sub>. Due to the salbutamol photodegradation, the degradation kinetic was slow in the first 60 min, referring to the transformation to intermediate compounds, and faster over the next 180 min of irradiation, referring the mineralization to small hydrocarbon fragments and carbon dioxide. The intermediate compounds including 2-(*tert*-butylamino)-1-(3,4-dihydroxyphenyl)ethanone, 2-(*tert*-butylamino)-ethanol and 2-(*tert*-butylamino)-1-(4-hydroxy-3-hydroxymethylphenyl)ethanone were first observed. Further, 2-(methylamino)-1-(3,4-dihydroxyphenyl)ethanone, 2-(*tert*-butylamino)-acetic acid, hydroquinone, and 1-(4-

hydroxyphenyl)ethanol were also detected after 180 min of irradiation. The photocatalytic degradation of pharmaceutical salbutamol was achieved in this study, and no toxic intermediate compounds were formed.

#### ■ ASSOCIATED CONTENT

##### Supporting Information

The Supporting Information is available free of charge at <https://pubs.acs.org/doi/10.1021/acsomega.3c01776>.

TEM images and plot of histogram for all samples and statistical analysis for particle size (PDF)

#### ■ AUTHOR INFORMATION

##### Corresponding Authors

**Auppatham Nakaruk** – Department of Industrial Engineering, Faculty of Engineering and Centre of Excellence for Innovation and Technology for Water Treatment, Faculty of Engineering, Naresuan University, Phitsanulok 65000, Thailand; [orcid.org/0000-0002-7399-5016](https://orcid.org/0000-0002-7399-5016); Email: [auppatham@nu.ac.th](mailto:auppatham@nu.ac.th)

**Wilawan Khanitchaidecha** – Department of Civil Engineering, Faculty of Engineering and Centre of Excellence for Innovation and Technology for Water Treatment, Faculty of Engineering, Naresuan University, Phitsanulok 65000, Thailand; Email: [wilawank1@gmail.com](mailto:wilawank1@gmail.com)

##### Authors

**Yumatorn Mingmongkol** – Department of Civil Engineering, Faculty of Engineering, Naresuan University, Phitsanulok 65000, Thailand

**Assadag Polnok** – Department of Pharmaceutical Technology, Faculty of Pharmaceutical Science, Naresuan University, Phitsanulok 65000, Thailand

**Patcharaporn Phuinthiang** – Department of Civil Engineering, Faculty of Engineering, Naresuan University, Phitsanulok 65000, Thailand; [orcid.org/0000-0001-6734-0470](https://orcid.org/0000-0001-6734-0470)

**Duangdao Channei** – Department of Chemistry, Faculty of Science, Naresuan University, Phitsanulok 65000, Thailand; [orcid.org/0000-0001-8951-3934](https://orcid.org/0000-0001-8951-3934)

**Khakhanang Ratananikom** – Department of Science and Mathematics, Faculty of Science and Health Technology, Kalasin University, Kalasin 46000, Thailand

Complete contact information is available at:  
<https://pubs.acs.org/10.1021/acsomega.3c01776>

## Notes

The authors declare no competing financial interest.

## ACKNOWLEDGMENTS

All of the authors would like to thank the late Dr. T.T.T. Dang, without whom this project would never have been possible. This work was supported by the Faculty of Engineering, Naresuan University's funding through the project R2566E002.

## REFERENCES

- (1) Hernández-Tenorio, R.; González-Juárez, E.; Guzmán-Mar, J. L.; Hinojosa-Reyes, L.; Hernández-Ramírez, A. WITHDRAWN: Review of occurrence of pharmaceuticals worldwide for estimating concentrations range in aquatic environments at the end of the last decade. *J. Hazard. Mater. Adv.* **2022**, *8*, 100137.
- (2) Zhao, H.; Zhou, J. L.; Zhang, J. Tidal impact on the dynamic behavior of dissolved pharmaceuticals in the Yangtze Estuary, China. *Sci. Total Environ.* **2015**, *536*, 946–954.
- (3) Chia, M. A.; Lorenzi, A. S.; Ameh, I.; Dauda, S.; Cordeiro-Araújo, M. K.; Agee, J. T.; Okpanachi, I. Y.; Adesalu, A. T. Susceptibility of phytoplankton to the increasing presence of active pharmaceutical ingredients (APIs) in the aquatic environment: A review. *Aquat. Toxicol.* **2021**, *234*, 105809.
- (4) Sakkas, V.; Calza, P.; Medana, C.; Villioti, A.; Baiocchi, C.; Pelizzetti, E.; Albanis, T. Heterogeneous photocatalytic degradation of the pharmaceutical agent salbutamol in aqueous titanium dioxide suspensions. *Appl. Catal., B* **2007**, *77*, 135–144.
- (5) Guo, B.; Sheng, W.; Yu, G.; Shi, M.; Deng, J.; Chen, W. Determination of salbutamol residue in pig muscle by direct competitive enzyme-linked immunosorbent assay. *Sci. Technol. Food Ind.* **2011**, *32*, No. e390.
- (6) Zhang, G.; Du, X.; Wang, Y.; Wang, H.; Wang, W.; Fu, Z. Controllable synthesis of SnS<sub>2</sub> nanostructures with high adsorption and photocatalytic activities. *Mater. Sci. Semicond. Process.* **2017**, *64*, 77–84.
- (7) Jallouli, N.; Elghniji, K.; Trabelsi, H.; Ksibi, M. Photocatalytic degradation of paracetamol on TiO<sub>2</sub> nanoparticles and TiO<sub>2</sub>/cellulosic fiber under UV and sunlight irradiation. *Arab. J. Chem.* **2017**, *10*, S3640–S3645.
- (8) Chaker, H.; Fourmentin, S.; Chérif-Aouali, L. Efficient Photocatalytic Degradation of Ibuprofen under Visible Light Irradiation Using Silver and Cerium Co-Doped Mesoporous TiO<sub>2</sub>. *ChemistrySelect* **2020**, *5*, 11787–11796.
- (9) Gang, R.; Xia, Y.; Xu, L.; Zhang, L.; Ju, S.; Wang, Z.; Koppala, S. Size controlled Ag decorated TiO<sub>2</sub> plasmonic photocatalysts for tetracycline degradation under visible light. *Surface. Interfac.* **2022**, *31*, 102018.
- (10) Razavi, F. S.; Ghanbari, D.; Dawi, E. A.; Salavati-Niasari, M. Electrospun bimetallic Au-Pt/TiO<sub>2</sub>/BaFe<sub>12</sub>O<sub>19</sub> nanofibers as promising photocatalysts driven by visible light: Synthesis and characterization. *J. Sci.: Adv. Mater. Devices* **2023**, *8*, 100559.
- (11) Zhang, J.; Zhai, M.; Wang, X.; Liu, S.; Zhang, L.; Liu, X.; Geng, Y.; Sun, X.; Liu, B. Pd nanoparticle-modified TiO<sub>2</sub>-x composites as efficient visible-light active photocatalysts for tetracycline degradation and microbial disinfection. *Opt. Mater.* **2023**, *136*, 113396.
- (12) Al-Gharibi, M. A.; Kyaw, H. H.; Al-Sabahi, J. N.; Zar Myint, M. T.; Al-Sharji, Z. A.; Al-Abri, M. Z. Silver nanoparticles decorated zinc oxide nanorods supported catalyst for photocatalytic degradation of paracetamol. *Mater. Sci. Semicond. Process.* **2021**, *134*, 105994.
- (13) Zia, J.; Riaz, U. Microwave-Assisted Degradation of Paracetamol Drug Using Polythiophene-Sensitized Ag–Ag<sub>2</sub>O Heterogeneous Photocatalyst Derived from Plant Extract. *ACS Omega* **2020**, *5*, 16386–16394.
- (14) Huang, D.; Li, J.; Zeng, G.; Xue, W.; Chen, S.; Li, Z.; Deng, R.; Yang, Y.; Cheng, M. Facile construction of hierarchical flower-like Z-scheme AgBr/Bi<sub>2</sub>WO<sub>6</sub> photocatalysts for effective removal of tetracycline: Degradation pathways and mechanism. *Chem. Eng. J.* **2019**, *375*, 121991.
- (15) Kitsiou, V.; Zachariadis, G. A.; Lambropoulou, D. A.; Tsiplakides, D.; Poullos, I. Mineralization of the antineoplastic drug carboplatin by heterogeneous photocatalysis with simultaneous synthesis of platinum-modified TiO<sub>2</sub> catalysts. *J. Environ. Chem. Eng.* **2018**, *6*, 2409–2416.
- (16) Rodger, B.; Baird, A. D. E.; Rice, E. W. *Standard Methods for the Examination of Water and Wastewater*; ED-Tech Press, 2017.
- (17) Nakaruk, A.; Kavei, G.; Sorrell, C. Synthesis of mixed-phase titania films by low-temperature ultrasonic spray pyrolysis. *Mater. Lett.* **2010**, *64*, 1365–1368.
- (18) Loan, T. T.; Long, N. N. Influence of Mn<sup>2+</sup> Doping on Structural Phase Transformation and Optical Property of TiO<sub>2</sub>: Mn<sup>2+</sup> Nanoparticles. *Commun. Phys.* **2019**, *29*, 251.
- (19) Chen, Y.; Yang, W.; Gao, S.; Sun, C.; Li, Q. Synthesis of Bi<sub>2</sub>MoO<sub>6</sub> Nanosheets with Rich Oxygen Vacancies by Postsynthesis Etching Treatment for Enhanced Photocatalytic Performance. *ACS Appl. Nano Mater.* **2018**, *1*, 3565–3578.
- (20) Nesbitt, H.; Banerjee, D. Interpretation of XPS Mn (2p) spectra of Mn oxyhydroxides and constraints on the mechanism of MnO<sub>2</sub> precipitation. *Am. Mineral.* **1998**, *83*, 305–315.
- (21) Ben khetta, O.; Attaf, A.; Derbali, A.; Saidi, H.; Bouhdjer, A.; Aida, M. S.; Ben khetta, Y.; Messemeche, R.; Nouadji, R.; Rahmane, S.; et al. Precursor concentration effect on the physical properties of transparent titania (Anatase-TiO<sub>2</sub>) thin films grown by ultrasonic spray process for optoelectronics application. *Opt. Mater.* **2022**, *132*, 112790.
- (22) Komaraiah, D.; Radha, E.; Sivakumar, J.; Ramana Reddy, M. V.; Sayanna, R. Photoluminescence and photocatalytic activity of spin coated Ag<sup>+</sup> doped anatase TiO<sub>2</sub> thin films. *Opt. Mater.* **2020**, *108*, 110401.
- (23) Amalraj, A.; Pius, A. Photocatalytic degradation of monocrotophos and chlorpyrifos in aqueous solution using TiO<sub>2</sub> under UV radiation. *J. Water Process Eng.* **2015**, *7*, 94–101.
- (24) Rao, T. P.; Kumar, M. S.; Angayarkanni, S. A.; Ashok, M. Effect of stress on optical band gap of ZnO thin films with substrate temperature by spray pyrolysis. *J. Alloys Compd.* **2009**, *485*, 413–417.
- (25) Zeng, M. Influence of TiO<sub>2</sub> surface properties on water pollution treatment and photocatalytic activity. *Bull. Korean Chem. Soc.* **2013**, *34*, 953–956.
- (26) Pinton, A. P.; Bulhões, L. O. d. S. Synthesis, characterization, and photostability of manganese-doped titanium dioxide nanoparticles and the effect of manganese content. *Mater. Res. Express* **2019**, *6*, 125015.
- (27) Dutton, B.; Woods, A.; Sadler, R.; Prime, D.; Barlow, D. J.; Forbes, B.; Jones, S. A. Using polar ion-pairs to control drug delivery to the airways of the lungs. *Mol. Pharm.* **2020**, *17*, 1482–1490.
- (28) Chandra Sekhar, M.; Purusottam Reddy, B.; Prabhakar Vattikuti, S.; Shanmugam, G.; Ahn, C.-H.; Park, S.-H. Structural, magnetic, and catalytic properties of Mn-doped titania nanoparticles synthesized by a sol-gel process. *J. Cluster Sci.* **2018**, *29*, 1255–1267.
- (29) Zhou, L.; Wang, Q.; Zhang, Y.; Ji, Y.; Yang, X. Aquatic photolysis of  $\beta$ -2-agonist salbutamol: kinetics and mechanism studies. *Environ. Sci. Pollut. Res.* **2017**, *24*, 5544–5553.